Proximity effect in a ferromagnetic semiconductor with spin-orbit interactions

Taketoki Yamashita,[1] Jaechul Lee,[1] Tetsuro Habe,[1] and Yasuhiro Asano[1,2]
[1]*Department of Applied Physics, Hokkaido University, Sapporo 060-8628, Japan*
[2]*Center of Topological Science and Technology, Hokkaido University, Sapporo 060-8628, Japan*

(Received 6 March 2019; revised manuscript received 14 August 2019; published 3 September 2019)

We study theoretically the proximity effect in a ferromagnetic semiconductor with the Rashba spin-orbit interaction. The interplay between the exchange potential and the spin-orbit interactions enriches the symmetry variety of Cooper pairs depending on degree of disorder in a ferromagnet. In the ballistic limit, spin-singlet *s*-wave Cooper pairs are the most dominant in the presence of strong spin-orbit interaction because the spin-momentum locking stabilizes a Cooper pair consisting of two electrons of time-reversal partner to each other. We will show that the spin-orbit interactions generate equal-spin-triplet *p*-wave pairs. In the dirty regime, on the other hand, equal-spin-triplet *s*-wave pairs are dominant because random impurity potentials release the locking. The exchange splitting in the conduction band causes the imbalance between two equal-spin pairing components. In a half-metallic ferromagnet, only an equal-spin pairing component survives and carries the spin-polarized supercurrent. We discuss the effects of the spin-orbit interaction on the Josephson current.

DOI: 10.1103/PhysRevB.100.094501

I. INTRODUCTION

The proximity effect into a ferromagnetic metal has been a central issue in physics of superconductivity [1–3]. The exchange potential in a ferromagnet enriches the symmetry variety of Copper pairs. The uniform exchange potential generates an opposite-spin-triplet Cooper pair from a spin-singlet *s*-wave Cooper pair. The pairing function of such opposite-spin pairs oscillates and decays spatially in the ferromagnet, which is the source of 0-π transition in a superconductor/ferromagnet/superconductor (SFS) junction [4–6]. The inhomogeneity in the magnetic moments near the junction interface induces equal-spin-triplet Cooper pairs which carries the long-range Josephson current in a SFS junction [3,7–11]. When the ferromagnet is in the diffusive transport regime, all the spin-triplet components belong to odd-frequency symmetry class [3,12–15].

An SFS junction consists of a ferromagnetic semiconductor may be a testing ground of spin-triplet Cooper pairs [16] because of its controllability of magnetic moments by doping. A long-range phase coherent effect is expected in such a high mobility two-dimensional electron gas on a semiconductor [17,18]. Indeed, an experiment has observed supercurrents flowing through a Nb/(In,Fe)As/Nb junction [19,20]. In addition, the spin configuration can be changed after fabricating the SFS junction through the Rashba spin-orbit interactions tuned by gating the ferromagnetic segment. It has been well established that the Rashba spin-orbit interaction generates the variation of spin structure in momentum space.

So far, the interplay between the exchange potential and the spin-orbit interaction in the proximity effect has been discussed in a number of theoretical studies [21–36]. This research area has attracted much attention since the proposal of topologically nontrivial superconducting nanowire [37,38]. A half-metallic quasi-one-dimensional nanowire can host Majorana fermions in its superconducting phase in the presence of spin-orbit interaction. The proximity effect of such a topologically nontrivial nanowire junction is simple. Namely, an odd-frequency equal-spin *s*-wave Cooper pair always plays a key role in the proximity effect of a material attached to the nontrivial nanowire [24]. In proximity structures consisting of a topologically trivial superconductor, on the other hand, symmetry of a Cooper pair can depend sensitively on the exchange potential, the spin-orbit potential, and the degree of disorder. The present paper addresses this issue.

In this paper, we study theoretically the symmetries of Cooper pairs in a two-dimensional ferromagnetic semiconductor with the Rashba spin-orbit interaction. The pairing function is calculated numerically by using the lattice Green's function technique on an SFS junction. The theoretical method can be applied to an SFS junction for arbitrary strength of the exchange potential, the spin-orbit interaction, and the interactions to random impurity potential. These potentials change the symmetry of a Cooper pair in a ferromagnet from spin-singlet *s*-wave symmetry in a superconductor. In the ballistic limit, spin-singlet *s*-wave Cooper pairs are the most dominant in the strong spin-orbit interaction because the spin-momentum locking stabilizes a Cooper pair consisting of two electrons of time-reversal partner to each other. We also find that the spin-orbit interactions generate equal-spin-triplet Cooper pairs belonging to odd-parity symmetry. The analytical results by solving the Eilenberger equation explains well the numerical results of pairing functions. In the presence of random impurities, equal-spin-triplet *s*-wave pairs are dominant in a diffusive ferromagnet. This conclusion remains unchanged even when the exchange potential is large enough to make a ferromagnet be half metallic. We also discuss effects of the spin-orbit interaction on the 0-π transition in an SFS junction.

This paper is organized as follows. In Sec. II, we explain the theoretical model of an SFS junction. The numerical results in the clean limit and those in a dirty regime are shown in Secs. III and IV, respectively. The conclusion is given in

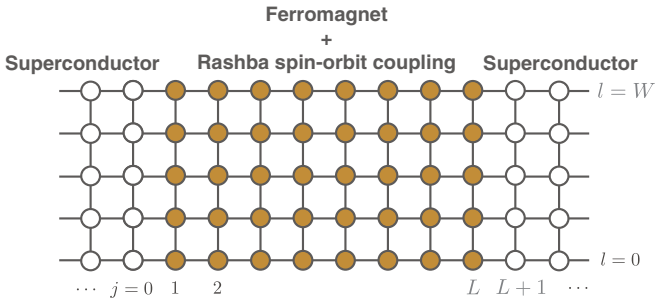

FIG. 1. SFS junction on two-dimensional tight-binding model.

Sec. V. We use the units of $\hbar = c = k_B = 1$ throughout this paper, where c is the speed of light and k_B is the Boltzmann constant.

II. MODEL

Let us consider an SFS junction on two-dimensional tight-binding lattice as shown in Fig. 1, where L is the length of the ferromagnetic semiconductor, W is the width of the junction in units of the lattice constant, $\boldsymbol{x}$ ($\boldsymbol{y}$) is the unit vector in the x (y) direction, $\boldsymbol{r} = j\boldsymbol{x} + m\boldsymbol{y}$ points to a lattice site. The Hamiltonian of the junction is given by

$$\mathcal{H} = \sum_{\boldsymbol{r},\boldsymbol{r}'} \Psi^\dagger(\boldsymbol{r}) \begin{bmatrix} \hat{H}_{\rm N}(\boldsymbol{r},\boldsymbol{r}') & \hat{\Delta}(\boldsymbol{r},\boldsymbol{r}') \\ -\hat{\Delta}^*(\boldsymbol{r},\boldsymbol{r}') & -\hat{H}^*_{\rm N}(\boldsymbol{r},\boldsymbol{r}') \end{bmatrix} \Psi(\boldsymbol{r}'), \quad (1)$$

$$\Psi(\boldsymbol{r}) = [\psi_\uparrow(\boldsymbol{r}), \psi_\downarrow(\boldsymbol{r}), \psi^\dagger_\uparrow(\boldsymbol{r}), \psi^\dagger_\downarrow(\boldsymbol{r})]^{\rm T}, \quad (2)$$

where $\psi_\alpha(\boldsymbol{r})$ is the annihilation operator of an electron with spin α at $\boldsymbol{r}$. The normal state Hamiltonian consists of four terms,

$$\hat{H}_{\rm N} = \hat{H}_{\rm k} + \hat{H}_{\rm so} + \hat{H}_{\rm h} + \hat{V}_{\rm i}, \quad (3)$$

$$\hat{H}_{\rm k}(\boldsymbol{r},\boldsymbol{r}') = -t(\delta_{\boldsymbol{r},\boldsymbol{r}'+\boldsymbol{x}} + \delta_{\boldsymbol{r}+\boldsymbol{x},\boldsymbol{r}'})\hat{\sigma}_0 - t(\delta_{\boldsymbol{r},\boldsymbol{r}'+\boldsymbol{y}} + \delta_{\boldsymbol{r}+\boldsymbol{y},\boldsymbol{r}'})\hat{\sigma}_0 + (4t - \epsilon_F)\delta_{\boldsymbol{r},\boldsymbol{r}'}\hat{\sigma}_0, \quad (4)$$

$$\hat{H}_{\rm so}(\boldsymbol{r},\boldsymbol{r}') = i(\lambda/2)[\{\delta_{\boldsymbol{r},\boldsymbol{r}'+\boldsymbol{x}} - \delta_{\boldsymbol{r}+\boldsymbol{x},\boldsymbol{r}'}\}\hat{\sigma}_2 - \{\delta_{\boldsymbol{r},\boldsymbol{r}'+\boldsymbol{y}} - \delta_{\boldsymbol{r}+\boldsymbol{y},\boldsymbol{r}'}\}\hat{\sigma}_1]\Theta(j)\,\Theta(L-j), \quad (5)$$

$$\hat{H}_{\rm h}(\boldsymbol{r},\boldsymbol{r}') = -\boldsymbol{h}\cdot\boldsymbol{\sigma}\,\delta_{\boldsymbol{r},\boldsymbol{r}'}\,\Theta(j)\,\Theta(L+1-j), \quad (6)$$

$$\hat{H}_{\rm i}(\boldsymbol{r},\boldsymbol{r}') = v_{\boldsymbol{r}}\,\sigma_0\,\delta_{\boldsymbol{r},\boldsymbol{r}'}\,\Theta(j)\,\Theta(L+1-j), \quad (7)$$

$$\hat{\Delta}(\boldsymbol{r},\boldsymbol{r}') = \Delta\,\delta_{\boldsymbol{r},\boldsymbol{r}'}\,i\,\hat{\sigma}_2[\Theta(-j+1)e^{i\varphi_L} + \Theta(j-L)e^{i\varphi_R}], \quad (8)$$

$$\Theta(j) = \begin{cases} 1 & : j > 1 \\ 0 & : j \leqslant 0, \end{cases} \quad (9)$$

where t is the hopping integral among the nearest-neighbor lattice sites, ϵ_F is the Fermi energy, $\hat{\sigma}_j$ for $j = 1-3$ and $\hat{\sigma}_0$ are the Pauli's matrix and unit matrix in spin space, respectively. In the ferromagnet ($1 \leqslant j \leqslant L$), λ is the amplitude of the spin-orbit interaction, $\boldsymbol{h}$ represents the uniform exchange potential, and $v_{\boldsymbol{r}}$ represents random impurity potential. In the two superconductors, Δ is the amplitude of the pair potential of spin-singlet s-wave symmetry, and $\varphi_L(\varphi_R)$ is the superconducting phase in the left (right) superconductor. The Hamiltonian in continuum is also given in Eq. (A1) in Appendix A.

We solve the Gor'kov equation,

$$\left[i\omega_n \hat{\tau}_0\hat{\sigma}_0 - \sum_{\boldsymbol{r}_1} \begin{pmatrix} \hat{H}_{\rm N}(\boldsymbol{r},\boldsymbol{r}_1) & \hat{\Delta}(\boldsymbol{r},\boldsymbol{r}_1) \\ -\hat{\Delta}^*(\boldsymbol{r},\boldsymbol{r}_1) & -\hat{H}^*_{\rm N}(\boldsymbol{r},\boldsymbol{r}_1) \end{pmatrix} \right] \times \check{G}_{\omega_n}(\boldsymbol{r}_1,\boldsymbol{r}') = \hat{\tau}_0\hat{\sigma}_0\delta(\boldsymbol{r}-\boldsymbol{r}'), \quad (10)$$

$$\check{G}_{\omega_n}(\boldsymbol{r},\boldsymbol{r}') = \begin{bmatrix} \hat{G}_{\omega_n}(\boldsymbol{r},\boldsymbol{r}') & \hat{F}_{\omega_n}(\boldsymbol{r},\boldsymbol{r}') \\ -\hat{F}^*_{\omega_n}(\boldsymbol{r},\boldsymbol{r}') & -\hat{G}^*_{\omega_n}(\boldsymbol{r},\boldsymbol{r}') \end{bmatrix}, \quad (11)$$

by applying the lattice Green's function technique [39,40], where τ_0 is the unit matrix in particle-hole space, $\omega_n = (2n+1)\pi T$ is the fermionic Matsubara frequency, and T is a temperature. The Josephson current in a ferromagnet $1 < j < L$ expressed as

$$J(j) = -\frac{ie}{2}\,T\sum_{\omega_n}\sum_{m=1}^{W} {\rm Tr}[\hat{\tau}_3\check{T}_+\,\check{G}_{\omega_n}(\boldsymbol{r},\boldsymbol{r}+\boldsymbol{x}) - \hat{\tau}_3\check{T}_-\,\check{G}_{\omega_n}(\boldsymbol{r}+\boldsymbol{x},\boldsymbol{r})], \quad (12)$$

$$\check{T}_\pm = \begin{bmatrix} -t\hat{\sigma}_0 \mp i(\lambda/2)\hat{\sigma}_2 & 0 \\ 0 & t\hat{\sigma}_0 \pm i(\lambda/2)\hat{\sigma}_2 \end{bmatrix}, \quad (13)$$

is independent of j.

The pairing function with s-wave symmetry is decomposed into four components,

$$\frac{1}{W}\sum_{m=1}^{W}\hat{F}_{\omega_n}(\boldsymbol{r},\boldsymbol{r}) = \sum_{\nu=0}^{3} f_\nu(j)\hat{\sigma}_\nu i\hat{\sigma}_2, \quad (14)$$

where f_0 is the spin-singlet component and f_j with $j = 1-3$ are the spin-triplet components. In the clean limit, we also calculate pairing function with an odd-parity symmetry

$$\frac{1}{2W}\sum_{m=1}^{W}\hat{F}_{\omega_n}(\boldsymbol{r}+\boldsymbol{x},\boldsymbol{r}) - \hat{F}_{\omega_n}(\boldsymbol{r}-\boldsymbol{x},\boldsymbol{r}) = \sum_{\nu=0}^{3} f_\nu(j)\hat{\sigma}_\nu i\hat{\sigma}_2. \quad (15)$$

Throughout this paper, we fix several parameters as $W = 20$, $\epsilon_F = 2t$, $\Delta = 0.005t$, and $T/T_c = 0.1$. The exchange field is always in the perpendicular direction to the two-dimensional plane $\boldsymbol{h} = h\boldsymbol{z}$. We do not consider self-consistency in the pair potential. In an experiment [20], the two-dimensional electron gas on a semiconductor is connected to the superconducting condensate in three-dimensional large superconductors. Thus, the superconducting order can be rigid in the superconductors independent of disordered potential and magnetic potentials in the semiconductor.

III. CLEAN LIMIT

A. Josephson current

We first discuss the numerical results of the Josephson current plotted as a function of the length of a ferromagnet L in Fig. 2, where we fix the phase difference at $\varphi = \varphi_L - \varphi_R = \pi/2$. Figures 2(a) and 2(b) show the results in the

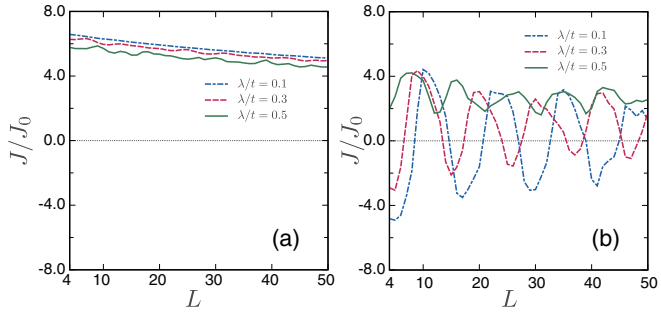

FIG. 2. The Josephson current versus the length of a normal segment L in the clean limit. (a) An SNS junction at $h = 0$. (b) An SFS junction at $h = 0.5t$.

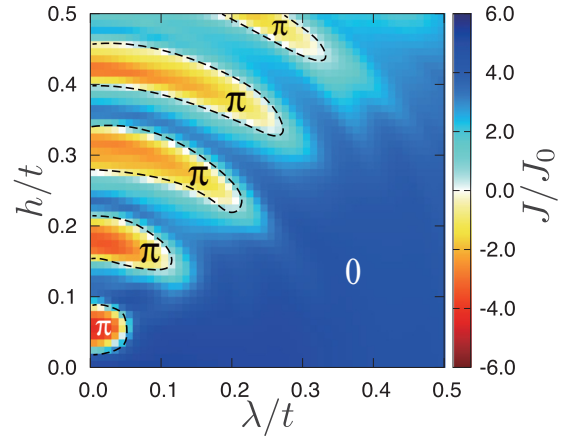

FIG. 3. The Josephson current at $\varphi = 0.5\pi$ and $L = 50$ is plotted as a function of h and λ in the clean limit.

absence of exchange potential $h = 0$ and in the presence of an exchange potential $h = 0.5t$, respectively. The Josephson current is normalized to $J_0 = e\Delta$ throughout this paper. The amplitude of the Josephson current slightly decreases with the increase of L because the pairing functions decay as e^{-x/ξ_T^C} with $\xi_T^C = v_F/2\pi T$ for all pairing symmetry [41]. The spin-orbit interaction affects the Josephson current in two different manners: The generation of spin-triplet Cooper pairs and the modification of normal conductance due to the band structure as shown in Fig. 6. In this paper, we mainly focus on the former effect which happens only when the spin-orbit interaction and the exchange potential coexist as shown in Sec. III C. Since $h = 0$ in Fig. 2(a), spin-triplet Cooper pairs are absent in a superconductor/normal-metal/superconductor (SNS) junction. The spin-orbit interactions modify the band structure as shown in Fig. 6 and decrease the transmission probability at the NS interface. The results in Fig. 2(a), however, demonstrate that such band effects on the normal conductance and on the Josephson current are very weak for $\lambda/t < 0.5$. On the other hand, in Fig. 2(b), the Josephson current oscillates as a function of L because of the exchange potential. The period of the oscillations is described by $\xi_h^C = v_F/2h$ in weak spin-orbit interactions. When the spin-orbit interaction increases, the amplitude of the oscillations decreases. At $\lambda = 0.5t$, the Josephson current is always positive at $\varphi = \pi/2$. In the present calculation at $T/T_c = 0.1$, the current-phase relationship (CPR) deviates slightly from sinusoidal function as

$$J = J_1 \sin(\varphi) - J_2 \sin(2\varphi), \tag{16}$$

with $J_2 > 0$. When $J_1 > 0$ ($J_1 < 0$), the junction is called 0 (π) junction. Roughly speaking, the spin-orbit interaction stabilizes the 0 state rather than the π state.

This conclusion can be confirmed by the results displayed in Fig. 3, where we show a phase diagram of the Josephson current at $\varphi = 0.5\pi$ and $L = 50$. The horizontal (vertical) axis indicates the amplitude of the spin-orbit interaction (exchange potential). The junction is in the 0 state for $J > 0$ and is in the π state for $J < 0$. At $\lambda = 0$, the Josephson current changes its sign with the increase of h, which indicates the 0-π transition by the exchange potential. When we introduce the spin-orbit interaction, the 0-π transition is suppressed [7,21,42] and the Josephson current is always positive at $\varphi = \pi/2$. The π state tends to disappear for $\lambda > h$. We will discuss the reasons for the disappearing π state under the strong spin-orbit interactions in Sec. III C.

B. Current-phase relationship

Before discussing the symmetry of a Cooper pair, the relation between the symmetry of the Hamiltonian and the CPR of the Josephson current should be clarified. The Hamiltonian of an SFS junction is described in continuum as shown in Eqs. (A1)–(A9) in Appendix A. The energy of a junction E depends on the phase difference between the two superconductors $\varphi = \varphi_L - \varphi_R$. The Josephson current is calculated by the relation $J(\varphi) = e\partial_\varphi E(\varphi)$. In the lowest order Josephson coupling, generally speaking, the current is expressed as

$$J = J_1 \sin(\varphi - \varphi_0), \tag{17}$$

where φ_0 is a phase shift. When a relation $E(\varphi) = E(-\varphi)$ is satisfied, the Josephson current is an odd function of φ, (i.e., $J(0) = 0$). As a result, φ_0 is either 0 or π. It is well known that an SNS (SIS) junction consisting of a conventional normal-metal (insulator) is always the 0 junction ($\varphi_0 = 0$). An SFS junction consisting of a uniform metallic ferromagnet (F) can be either 0 junction or π junction ($\varphi_0 = \pi$), depending on the length of a ferromagnet and the amplitude of the exchange potential [1,4]. The φ_0 junction is the Josephson junction with φ_0 being neither 0 nor π. It has been known that such a φ_0 state is realized in an SFS junction consisting of a ferromagnet with inhomogeneous magnetic moments [13,43,44] and a ferromagnet with spin-orbit interactions [22,29]. Although spin-orbit interaction is present in the ferromagnet in our study, φ_0 in Fig. 3 it is limited to be either 0 or π. We explain the reasons in what follows.

The transformation of $\varphi \to -\varphi$ is realized by applying the complex conjugation to the Hamiltonian in Eq. (A2). Therefore, the junction energy satisfies $E(\varphi) = E(-\varphi)$ when

$$H_{\rm p} = H_{\rm p}^*, \tag{18}$$

where we consider $H_{\rm i}=0$ in the ballistic limit and the magnetic moment is in the z direction $h\hat{\sigma}_3$. The potentials in this paper are represented as

$$H_{\rm p}=h\hat{\sigma}_3-i\lambda\partial_y\sigma_1+i\lambda\partial_x\sigma_2, \tag{19}$$

$$H_{\rm p}^{*}=h\hat{\sigma}_3+i\lambda\partial_y\sigma_1+i\lambda\partial_x\sigma_2. \tag{20}$$

Although the second term changes it sign under the complex conjugation, the additional transformation $y\to -y$ cancels the sign changing. Therefore the Hamiltonian preserves

$$H_{\rm p}^{*}(x,-y)=H_{\rm p}(x,y). \tag{21}$$

In this transformation, the space coordinate is transformed as $(x,y,z)\to(x,-y,z)$ and spin is transformed as $(\sigma_1,\sigma_2,\sigma_3)\to(\sigma_1,-\sigma_2,\sigma_3)$. The invariance of the Hamiltonian under such transformation is called magnetic mirror reflection (MMR) symmetry with respect to the xz plane [35]. Thus, $E(\varphi)$ in our junction is an even function of φ and the junction is either 0 or π state as shown in Appendix A. The previous papers [23,29] demonstrated that the Zeeman filed in the y direction generates the phase shift φ_0. In these cases, $H_{\rm h}'=h_y\hat{\sigma}_2$ changes its sign under the complex conjugation. Breaking MMR symmetry by h_y explains the mechanism of the tunable feature of φ_0. The previous papers [28,45] explain such phase shifts in terms of SU(2) magnetic field. In Fig. 3, the magnetic moment is in the z direction. The paper in Ref. [29] also showed that φ_0 is either 0 or π when the Zeeman field is in the x direction. The Zeeman field in the xz plane does not cause the phase shift because it preserves MMR symmetry.

C. Pairing functions

To analyze the characteristic behavior of the Josephson current, we solve the Eilenberger equation [46] in a ferromagnet:

$$iv_F\hat{\boldsymbol{k}}\cdot\boldsymbol{\nabla}_{\boldsymbol{r}}\check{g}+[\check{H}_0+\check{\Delta},\check{g}]_-=0, \tag{22}$$

$$\check{H}_0=(i\omega_n-\boldsymbol{h}\cdot\hat{\boldsymbol{\sigma}})\hat{\tau}_3-\boldsymbol{\lambda}\times\hat{\boldsymbol{\sigma}}\cdot\hat{\boldsymbol{k}}, \tag{23}$$

$$\check{\Delta}=i\hat{\Delta}\hat{\tau}_1. \tag{24}$$

In the Bogoliubov-de Gennes (BdG) Hamiltonian, the spin-orbit interaction is described by

$$H_{\rm SO}=\tilde{\boldsymbol{\lambda}}\times\hat{\boldsymbol{\sigma}}\cdot(-i\boldsymbol{\nabla}). \tag{25}$$

We apply the quasiclassical approximation to this term and derive the second term in Eq. (23), where $\boldsymbol{\lambda}$ is a vector with the energy dimension and $\hat{\boldsymbol{k}}$ is the unit vector on the Fermi surface. Generally speaking, the quasiclassical approximation is valid when the Fermi energy is much larger than other energy scales such as Δ, $|\boldsymbol{h}|$, and $|\boldsymbol{\lambda}|$. To solve the Eilenberger equation, we apply the Riccati parametrization,

$$\check{g}=\begin{pmatrix}\hat{N} & \hat{0}\\ \hat{0} & \underline{\hat{N}}\end{pmatrix}\begin{pmatrix}s_{\omega_n}(1-\hat{a}\underline{\hat{a}}) & 2\hat{a}\\ 2\underline{\hat{a}} & -s_{\omega_n}(1-\underline{\hat{a}}\hat{a})\end{pmatrix}, \tag{26}$$

where $s_{\omega_n}=\mathrm{sgn}(\omega_n)$ and $\hat{N}=(1+\hat{a}\,\underline{\hat{a}})^{-1}$. The two Riccati parameters are related to each other by $\underline{\hat{a}}(\boldsymbol{r},\hat{\boldsymbol{k}},i\omega_n)=\hat{\sigma}_2\hat{a}^{*}(\boldsymbol{r},-\hat{\boldsymbol{k}},i\omega_n)\hat{\sigma}_2$. Here we show the relation between the Ricatti parameter in Eq. (26) and anomalous Green's function $\hat{F}$ in the Gor'kov equation [47]:

$$\hat{f}(\boldsymbol{r},\hat{\boldsymbol{k}},i\omega_n)=\frac{i}{\pi}\int d\xi_k\hat{F}(\boldsymbol{r},\boldsymbol{k},i\omega_n), \tag{27}$$

$$=i2\hat{N}(\boldsymbol{r},\hat{\boldsymbol{k}},i\omega_n)\,\hat{a}(\boldsymbol{r},\hat{\boldsymbol{k}},i\omega_n)\hat{\sigma}_2, \tag{28}$$

$$\hat{a}(\boldsymbol{r},\hat{\boldsymbol{k}},i\omega_n)=\sum_{\nu=0}^{3}a_\nu(\boldsymbol{r},\hat{\boldsymbol{k}},i\omega_n)\hat{\sigma}_\nu. \tag{29}$$

The spin-singlet component satisfies

$$a_0(\boldsymbol{r},\hat{\boldsymbol{k}},i\omega_n)=a_0(\boldsymbol{r},-\hat{\boldsymbol{k}},-i\omega_n), \tag{30}$$

and the three spin-triplet components satisfy

$$a_j(\boldsymbol{r},\hat{\boldsymbol{k}},i\omega_n)=-a_j(\boldsymbol{r},-\hat{\boldsymbol{k}},-i\omega_n) \tag{31}$$

for $j=1-3$. The Riccati parameter obeys

$$\begin{aligned}&iv_F\hat{\boldsymbol{k}}\cdot\boldsymbol{\nabla}\hat{a}+2i\omega_n\hat{a}-\boldsymbol{h}\cdot\hat{\boldsymbol{\sigma}}\hat{a}-\hat{a}\hat{\boldsymbol{\sigma}}\cdot\boldsymbol{h}-\hat{\boldsymbol{k}}\times\boldsymbol{\lambda}\cdot\hat{\boldsymbol{\sigma}}\hat{a}\\&\quad+\hat{a}\hat{\boldsymbol{k}}\times\boldsymbol{\lambda}\cdot\hat{\boldsymbol{\sigma}}-i\Delta+i\hat{a}\Delta\hat{a}=0.\end{aligned} \tag{32}$$

In what follows, we solve Eq. (32) in a ferromagnet of a SF junction, where a ferromagnet ($x>0$) is attached a superconductor at $x=0$. We assume that the junction is translational invariant in the y direction. Since $\Delta=0$ in the ferromagnet, it is possible to have an analytic solution of $\hat{a}(\boldsymbol{r},\hat{\boldsymbol{k}},i\omega_n)$.

For $\boldsymbol{h}=hz$ and $\boldsymbol{\lambda}=\lambda z$, we obtain the solution in two dimensions,

$$a_0=\frac{A_0}{V^2}\left[h^2\cos\left(\frac{2V}{v_{F_x}}x\right)+\lambda^2\right]e^{-\frac{2\omega_n}{v_{F_x}}x}, \tag{33}$$

$$a_{\uparrow\uparrow}=a_1-ia_2, \tag{34}$$

$$=\frac{A_0h\lambda}{V^2}(\hat{k}_y+i\hat{k}_x)\left[1-\cos\left(\frac{2V}{v_{F_x}}x\right)\right]e^{-\frac{2\omega_n}{v_{F_x}}x}, \tag{35}$$

$$a_{\downarrow\downarrow}=a_1+ia_2, \tag{36}$$

$$=\frac{A_0h\lambda}{V^2}(-\hat{k}_y+i\hat{k}_x)\left[1-\cos\left(\frac{2V}{v_{F_x}}x\right)\right]e^{-\frac{2\omega_n}{v_{F_x}}x}, \tag{37}$$

$$a_3=i\frac{A_0h}{V}\sin\left(\frac{2V}{v_{F_x}}x\right)e^{-\frac{2\omega_n}{v_{F_x}}x}, \tag{38}$$

where $V=\sqrt{h^2+\lambda^2}$, $v_{F_x}=k_x/m$ and $A_0=\Delta/(|\omega_n|+\sqrt{\omega_n^2+\Delta^2})$ is the solution in a uniform superconductor. At the interface of a superconductor and a ferromagnet ($x=0$), we imposed a boundary condition of $a_0=A_0$ and $a_j=0$ for $j=1-3$. The decay length of all the components is basically given by the thermal coherence in the clean limit $\xi_T^C=v_F/2\pi T$. The spin-singlet component a_0 has two contributions: An oscillating term due to the exchange potential and a constant term due to the spin-orbit interaction. Equations (33)–(38) suggest that only a spin-singlet pair stays in an SNS junction with $h=0$. Thus the spin-orbit interaction does not affect the Josephson current so much as shown in Fig. 2(a). As shown in Eq. (38), the exchange potential generates the opposite-spin-triplet component a_3 which oscillates in real space. The equal-spin pairing components $a_{\uparrow\uparrow}$ and $a_{\downarrow\downarrow}$ become finite when the spin-orbit interaction and the exchange potential coexist. Although $a_{\sigma,\sigma}$ components osculate in real

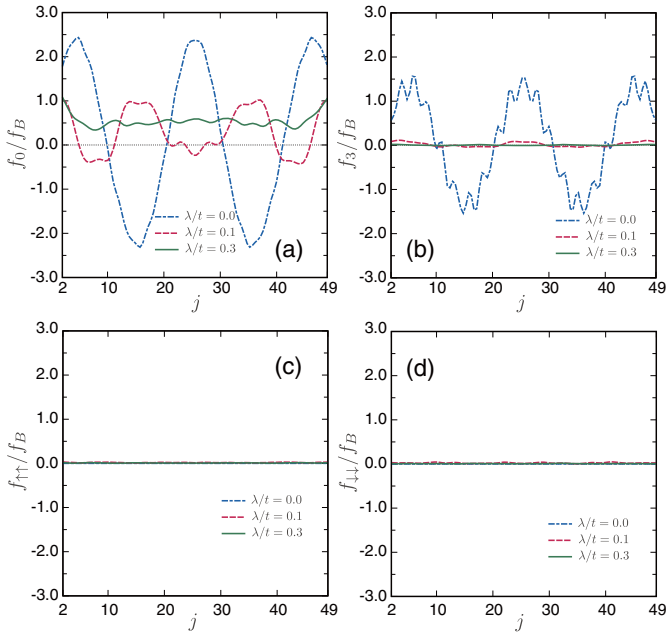

FIG. 4. The spatial profile of the pairing functions at $L = 50$ and $h = 0.3t$ in the clean limit. The results for an s-wave symmetry in Eq. (14) are presented. (a) Spin-singlet f_0, (b) opposite-spin-triplet f_3, (c) equal-spin-triplet $f_{\uparrow\uparrow}$, and (d) equal-spin-triplet $f_{\downarrow\downarrow}$.

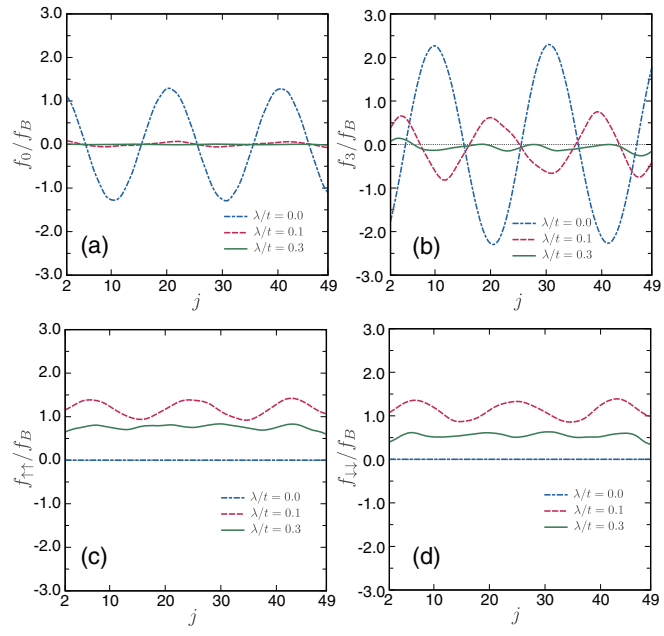

FIG. 5. The results for an odd-parity symmetry in Eq. (15). The parameters are the same with those in Fig. 4. (a) Spin-singlet f_0, (b) opposite-spin-triplet f_3, (c) equal-spin-triplet $f_{\uparrow\uparrow}$, and (d) equal-spin-triplet $f_{\downarrow\downarrow}$.

space, they do not change their signs as shown in Eqs. (35) and (37).

In Fig. 4, we show the numerical results of pairing function in the ferromagnet of an SFS junction on the tight-binding model, where $L = 50$, $\varphi = 0$, $h = 0.3t$, and $\omega_n = 0.02\Delta$. The pairing function is normalized to f_B, which is the amplitude of the anomalous Green's function in the uniform superconductor. We first display the spatial profile of s-wave components defined in Eq. (14) for several choices of λ. The spin-singlet s-wave component f_0 in Fig. 4(a) oscillates and changes its sign in real space at $\lambda = 0$. However, the spin-orbit interaction suppresses the sign change. As a result, f_0 is positive everywhere for $\lambda = 0.3t$. The opposite-spin-triplet component f_3 in Fig. 4(b) always changes its sign but is strongly suppressed by the spin-orbit interactions. We note that f_3 belongs to odd-frequency spin-triplet even-parity (OTE) symmetry class. The two equal-spin-triplet components in Figs. 4(c) and 4(d) are absent irrespective of λ. The analytical results of the Eilenberger equation in Eqs. (33)–(38) predict these behaviors well. A previous paper [36] has discussed the similar effect in a SFS junction with the spin-orbit interaction working at the thin ferromagnetic layer. Namely, the amplitude of all OTE components are much smaller than that of spin-singlet s-wave component in the presence of the spin-orbit interaction. However, little attention has been given to odd-parity pairing correlations. The generation of odd-parity components is an essential effect of the spin-orbit interaction as shown in Fig. 5, where we display the spatial profile of the odd-parity components in Eq. (15) for several choices of λ. Odd-parity opposite-spin Cooper pairs are generated in the clean junction because the exchange potential breaks inversion symmetry locally at the junction interface. The spin-singlet p-wave component f_0 in Fig. 5(a) oscillates and changes its sign in real space at $\lambda = 0$. The spin-orbit interaction drastically suppresses such an odd-frequency spin-singlet odd-parity component. The opposite-spin-triplet component f_3 in Fig. 5(b) belonging to even-frequency spin-triplet odd-parity class shows the similar behavior to f_0. Finally, the spin-orbit interactions generate two equal-spin-triplet components $f_{\uparrow\uparrow}$ and $f_{\downarrow\downarrow}$ as shown in Figs. 5(c) and 5(d), respectively. They oscillate slightly in real space but do not change their sign. Together with Eqs. (35) and (37), equal-spin pairs generated by the spin-orbit interaction belong to p-wave symmetry. Together with Figs. 4(c) and 4(d), we conclude that equal-spin Cooper pairs belong to p-wave symmetry in a ballistic junction. The amplitude of such odd-parity equal-spin components first increases with the increase of λ, then decrease in agreement with the analytical results in Eqs. (35) and (37). We will explain the reasons of the reentrant behavior in what follows.

Figure 6 shows the schematic spin structure on the Fermi surface. When the exchange potential is much larger than the spin-orbit interactions, spin of an electron aligns in each spin band. The spin-orbit interactions twist the spin structure as shown in the upper middle figure. The strong spin-orbit interactions cause the spin-momentum locking as shown in the upper right figure. The spin configuration in the two limits are shown in the lower figure. The wave number $k_\pm$ in the figure are $k_\pm = k_F \pm h/v_F$ in the limit of $h \gg \lambda$ on the left and $k_\pm = k_F \pm \lambda/v_F$ in the limit of $h \ll \lambda$ on the right. At $h \gg \lambda$, a spin-singlet pair and an opposite-spin-triplet pair have a center-of-mass-momentum of $k_+ + (-k_-) = 2h/v_F$ on the Fermi surface. As a result, these components oscillate and change their signs in real space [48,49]. On the other hand, equal-spin-triplet components $f_{\uparrow\uparrow}$ ($f_{\downarrow\downarrow}$) do not have a center-of-mass-momentum because they consist of two electrons at $\pm k_+$ ($\pm k_-$). Thus equal-spin-triplet components do not

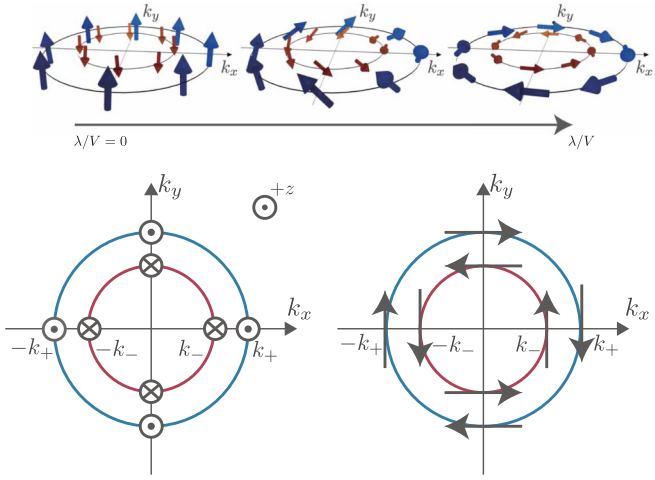

FIG. 6. Schematic picture of spin configuration on the Fermi surface. In the upper figure, the spin of an electron is twisted by the spin-orbit interaction on the Fermi surface. The strong spin-orbit interaction fells the spin down to the two-dimensional plane. In the lower figure, spin configuration on the two Fermi surfaces are shown for the two limits: $h \gg \lambda$ on the left panel and $h \ll \lambda$ on the right panel.

change signs as shown in the results for $\lambda = 0.1t$ in Figs. 5(c) and 5(d).

In the opposite limit of $h \ll \lambda$, a spin-singlet Cooper pair does not have a center-of-mass-momentum in this case. The spin-momentum locking due to strong spin-orbit interactions stabilizes such a Cooper pair consisting of two electrons of the time-reversal partner. Thus f_0 does not change its sign as shown in the results for $\lambda = 0.3t$ in Fig. 4(a). Equal-spin-triplet pairs, on the other hand, have the center-of-mass-momentum $2\lambda/v_F$. In Figs. 5(c) and 5(d), $f_{\sigma\sigma}$ for $\lambda = 0.1t$ oscillates in real space. Since the spatial oscillations cost the energy, $f_{\sigma\sigma}$ for $\lambda = 0.3t$ is smaller than that for $\lambda = 0.1t$. All the dominant pairing components do not change their sign. Therefore, the 0 state is more stable than the π state for $\lambda > h$ as shown in Fig. 3.

IV. DIRTY REGIME

In the dirty limit, we switch on the random impurity potential in Eq. (7) in a ferromagnet, where the potential is given randomly in the range of $-V_{\rm imp}/2 \leqslant v_{\boldsymbol{r}} \leqslant V_{\rm imp}/2$. In the numerical simulation, we set $V_{\rm imp} = 2t$, which results in the mean-free path ℓ about five lattice constants. Since $\ell \ll L$, a ferromagnet is in the diffusive transport regime. The coherence length $\xi_0 = v_F/\pi\Delta$ is estimated as 20 lattice constants at $\Delta = 0.005t$. Thus the junction is in the dirty regime because of $\ell < \xi_0$. The Josephson current is first calculated for a single sample with a specific random impurity configuration. Then the results are averaged over $N_{\rm s}$ samples with different impurity configurations:

$$\langle J \rangle = \frac{1}{N_{\rm s}} \sum_{i=1}^{N_{\rm s}} J_i. \tag{39}$$

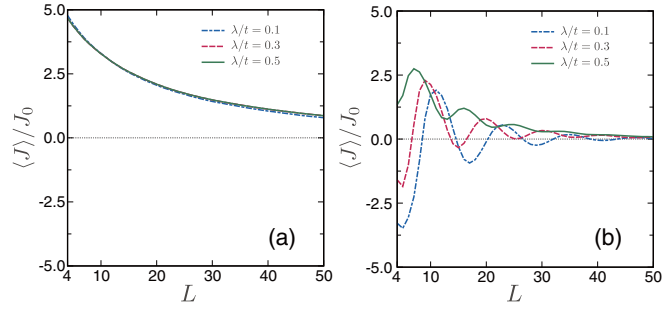

FIG. 7. The Josephson current versus the length of a normal segment L in the dirty limit. (a) An SNS junction at $h = 0$. (b) An SFS junction at $h = 0.5t$. The parameters here are the same as those in Fig. 2.

In this paper, we choose $N_{\rm s}$ as 100–500 in numerical simulation. We confirmed that the CPR of ensemble averaged Josephson current is sinusoidal and the shift φ_0 in Eq. (17) is either 0 or π. We will discuss the details of the CPR in Sec. IV B.

A. Josephson current

In Fig. 7, we show the ensemble average of the Josephson current as a function of the length of the ferromagnet, where we fix $\varphi = \pi/2$, the exchange potential is absent in Fig. 7(a) and the exchange potential is $h = 0.5t$ in Fig. 7(b). The decay length of the Josephson current in Fig. 7(a) is shorter than that in the clean limit in Fig. 2(a). It is well known in a diffusive normal metal that the penetration length of a Cooper pairs is limited by $\xi_T^D = \sqrt{D/2\pi T}$. In the absence of the exchange potential, spin-triplet pairs are absent in a SNS junction. The spin-orbit interactions only modify the band structure as shown in Fig. 6, which decreases the transmission probability at the junction and the amplitude of Josephson current. The Josephson current in Fig. 7(a) is almost independent of λ. The results suggest that the impurity scatterings wash out such band effect for $\lambda/t < 0.5$. The results of an SFS junction in Fig. 7(b) show the oscillations and the sign change of the Josephson current at $\lambda = 0.1t$. The large spin-orbit interaction suppresses the sign change of the Josephson current as show in the result for $\lambda = 0.3t$.

In Fig. 8, we plot the ensemble average of Josephson current at $\varphi = \pi/2$ as a function of h and λ. The results should be compared with those in Fig. 3. The amplitude of the Josephson current is suppressed by the impurity scatterings. Although the 0-π transition can be seen at $\lambda = 0$, the spin-orbit interaction suppresses the 0-π transition. Although such tendency is common at the results in the clean limit in Figs. 3 and those at a dirty regime in Fig. 8, symmetries of Cooper pairs carrying the Josephson current are different in the two cases. We will address this issue in Sec. IV C.

B. Current-phase relationship

Before discussing symmetry of Cooper pairs, we briefly explain an unusual property of CPR in the dirty regime. As already mentioned in Sec. III B, the phase shift φ_0 is either 0 or π in the clean limit because of MMR symmetry described by

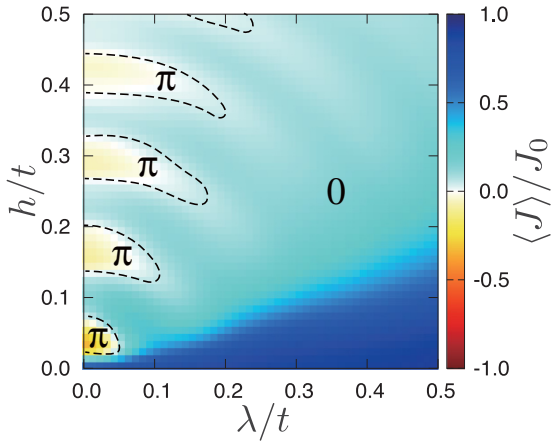

FIG. 8. The Josephson current is plotted as a function of h and λ in the dirty regime. The parameters are the same as those in Fig. 3.

the relation Eq. (21). In the presence of impurities, the random impurity potential $H_{\rm i}$ enters $H_{\rm P}$ in Eq. (A6). In such case, the relation Eq. (21) does not hold true because the random potential should be

$$H_{\rm i}(x,-y) \neq H_{\rm i}(x,y). \tag{40}$$

Namely, impurity potential breaks MMR symmetry, which results in a phase shift φ_i in the Josephson current in a single sample:

$$J_i = J_{1,i}\sin(\varphi-\varphi_i). \tag{41}$$

The shift φ_i is not predictable because it depends on a microscopic configuration of random impurities. The numerical results of the CPR for several samples are shown in Fig. 11 in Appendix B with broken lines, where $h = 0.5t$ and $\lambda = 0.5t$. The results show that the phase shift φ_i can be either positive or negative depending on random distribution. However, the ensemble average of the results shows the phase shift is zero as plotted with a thick line in Fig. 11. The ensemble average of the impurity potential $\langle H_{\rm i}(\boldsymbol{r})\rangle$ is independent of $\boldsymbol{r}$. Thus the Hamiltonian after averaging recovers MMR symmetry.

Here we briefly discuss a relation between the Josephson current in theories and that in experiments. In experiments, the Josephson current is measured in a specific sample of SFS junction. Since the Josephson effect is a result of the phase coherence of a quasiparticle in a ferromagnet, the Josephson current is not a self-averaged quantity. Therefore, the Josephson current calculated theoretically at a single sample J_i corresponds to that measured experimentally at a single junction. When $\langle J\rangle$ and J_i show qualitatively different behavior from each other, $\langle J\rangle$ cannot predict a Josephson current measured in experiments [40]. A previous paper [23] has discussed the phase shift φ_0 due to the Zeeman field in the y direction. In a specific junction in an experiment, an extra phase shift due to random potential in the junction may damage the controllability of φ_0 value. The numerical results in Fig. 11, however, show that φ_i is much smaller than π and that the amplitude of the Josephson current in a single sample is described well by the amplitude after averaging. The Josephson current has such property in a wide parameter range of exchange potential and the spin-orbit interaction. In the dirty limit, therefore, the results presented in previous papers [28,32,45] could predict the amplitude of the Josephson current.

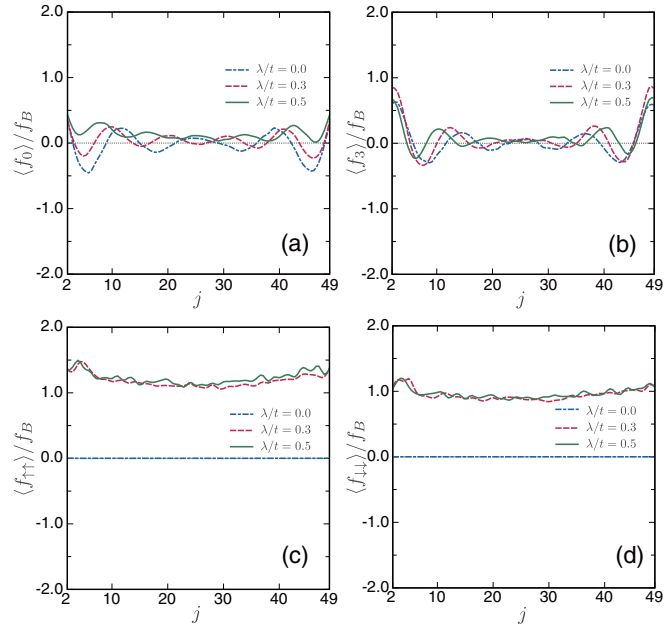

FIG. 9. The spatial profile of the ensemble average of pairing function in the dirty regime. Only an s-wave component remains finite in the dirty regime. The parameters are the same as those in Fig. 4.

C. Pairing functions

Although the ensemble average of the Josephson current in theories cannot predict the CPR measured in a real sample, the ensemble average of the pairing functions tells us characteristic features of the proximity effect. In Fig. 9, we show the spatial profile of the pairing functions in dirty regime, where $\varphi = 0$, $h_z = 0.5t$ and $L = 50$. The parameters here are the same as those in Fig. 4. The singlet component $\langle f_0\rangle$ oscillates and changes its sign at $\lambda = 0$ as shown in Fig. 9(a). At $\lambda = 0.5t$, the spin-orbit interaction suppress the amplitude of oscillations. The similar tendency can be found in the opposite-spin-triplet component $\langle f_3\rangle$ in Fig. 9(b). The equal-spin-triplet components $\langle f_{\sigma\sigma}\rangle$ are zero at $\lambda = 0$. The amplitudes of such OTE pairs become finite and spatially uniform in the dirty regime as shown in Figs. 9(c) and 9(d). The presence of odd-frequency pairs causes the enhancement of the local density of states at zero energy, which was confirmed by the previous papers [30,32] and is the source of the orbital paramagnetic response [50,51]. Such characteristic features in the pairing functions can be seen also in a single sample shown in Fig. 12 in Appendix B. Although the results in a single sample show aperiodic oscillations due to random impurity potential, $f_{\sigma\sigma}$ in a single sample are positive everywhere as shown in Figs. 12(c) and 12(d).

In the clean limit, the spin-momentum locking suppresses the equal-spin-triplet components as shown in Figs. 5(c) and 5(d). Actually, $f_{\sigma\sigma}$ first increases with the increase of λ, then decreases. In the dirty regime, however, the random impurity scatterings release the spin-momentum locking because the

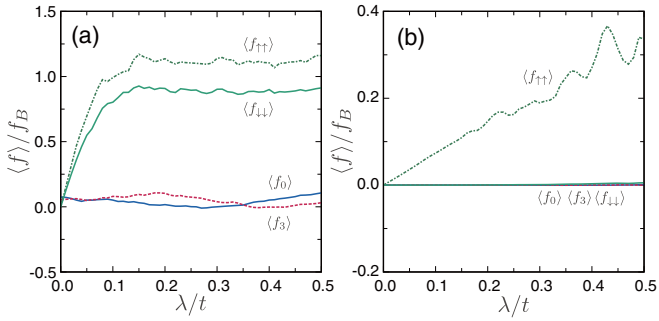

FIG. 10. The pairing functions at the center of a ferromagnet $j = 25$ are shown as a function of λ. (a) A strong ferromagnet at $h = 0.5t$. (b) A half-metallic ferromagnet at $h = 2.5t$.

momentum is not a good quantum number. As a result, the spin-orbit interactions flip the spin of $\langle f_3\rangle$ component and generates $\langle f_{\sigma\sigma}\rangle$ component without changing its parity. The resulting equal-spin Cooper pairs belong to odd-frequency equal-spin-triplet s-wave (OTE) symmetry class and have the long-range property in the ferromagnet [3]. At $\lambda > h$, the results in Fig. 9 show that equal-spin pairs are much more dominant than opposite-spin pairs.

We fix $j = 25$ in Fig. 9 at a center of a ferromagnet and calculate the pairing functions as a function of λ. The results are presented in Fig. 10, where we choose $h = 0.5t$ as a strong ferromagnet in Fig. 10(a) and $h = 2.5t$ as a half-metal in Fig. 10(b). The pairing functions of opposite-spin pair $\langle f_0\rangle$ and $\langle f_3\rangle$ are insensitive to λ. The amplitude of equal-spin pairs $\langle f_{\sigma\sigma}\rangle$ increases with the increase of λ and saturate for $\lambda > 0.2t$ in Fig. 10(a) as suggested already by previous papers [26,32]. These papers predicted the presence of an odd-frequency equal-spin s-wave pairs in a strong ferromagnet based on the solution of the quasiclassical Usadel equation. Since the applicability of the Usadel equation is limited to weak ferromagnets, we confirm their prediction by the numerical simulation beyond the quasiclassical approximation.

When we increase the exchange potential to $h = 2.5t$ in Fig. 10(b), a ferromagnet becomes half metallic. Namely, the ferromagnet is metallic for a spin-↑ electron and is insulating for a spin-↓ electron. Equal-spin Cooper pairs in Fig. 9 are formed in two steps under the coexistence of the exchange potential, the spin-orbit interaction and impurities. At the first step, the magnetic moment generates an opposite-spin-triplet s-wave Cooper pair from a spin-singlet s-wave pair. At the second step, the spin-orbit interaction flips spin of an opposite-spin-triplet pair and converts it to an equal-spin-triplet s-wave pair in the dirty case. However, it has been unclear if the spin-orbit interaction would be able to generate an equal-spin pair in a half metal because neither a spin-singlet pair nor an opposite-spin triplet pair can penetrate into it. The results in Fig. 10(b) show clearly the existence of an odd-frequency equal-spin Cooper pair $\langle f_{\uparrow\uparrow}\rangle$ in a half metal. The almost linear relationship between λ and $\langle f_{\uparrow\uparrow}\rangle$ suggests that the amplitude of odd-frequency pairs is controllable by tuning λ in experiments.

The presence of an equal-spin pair for only one spin-direction is a characteristic feature of the proximity effect in a half metal [3,8–14]. The spin-orbit interactions generate an equal-spin pair in the theoretical model in this paper, whereas inhomogeneous magnetic configuration at the junction interface generate an equal-spin pair in real half-metallic SFS junctions [3,8,9]. In these SFS junctions, $\langle f_{\uparrow\uparrow}\rangle$ component carries the usual Josephson current characterized by the sinusoidal CPR. In a topologically nontrivial nanowire junction [37,38], $\langle f_{\uparrow\uparrow}\rangle$ component in a half-metallic nanowire causes the anomalous Josephson effect characterized by the fractional CPR at a low temperature [24]. The dependence of $\langle f_{\uparrow\uparrow}\rangle$ on the Matsubara frequency is qualitatively different in the two cases. Namely, $\langle f_{\uparrow\uparrow}\rangle$ is analytic at $\omega_n = 0$ in the present junction, whereas it is singular like ω_n^{-1} in the topologically nontrivial junction. Tuning ω_n dependence of $\langle f_{\uparrow\uparrow}\rangle$ would be a next issue toward controlling Majorana bound states.

V. CONCLUSION

We theoretically study the proximity effect at a ferromagnetic semiconductor with the Rashba spin-orbit interaction by solving the Gor'kov equation on a two-dimensional tight-binding lattice. The Green's function is obtained numerically by using the lattice Green's function technique. The exchange potential in a ferromagnet converts a spin-singlet Cooper pair to an opposite-spin-triplet Cooper pair. The spin-orbit interactions generate an equal-spin-triplet Cooper pair from an opposite-spin-triplet Cooper pair. The relative amplitudes of the four spin-pairing components depend on the amplitude of spin-orbit interaction and the transport regime in a ferromagnet. In the presence of strong spin-orbit interaction, the spin-momentum locking stabilizes a conventional spin-singlet s-wave Cooper pair in the ballistic limit. Under the weak spin-orbit interaction, equal-spin-triplet p-wave Cooper pairs appear as a subdominant pairing correlation. In the dirty regime, on the other hand, the most dominant Cooper pair in a ferromagnet belongs to an odd-frequency equal-spin-triplet s-wave symmetry class. The impurity scatterings release the spin-momentum locking in the dirty regime. We also numerically confirm the existence of an equal-spin-triplet in a dirty half-metallic ferromagnet.

ACKNOWLEDGMENTS

The authors are grateful to Y. Fominov, T. Nakamura, Y. Tanaka, and A. A. Golubov for useful discussions. This work was supported by Topological Materials Science (No. JP15H05852) from the Ministry of Education, Culture, Sports, Science and Technology (MEXT) of Japan, JSPS Core-to-Core Program (A. Advanced Research Networks), and Japanese-Russian JSPS-RFBR Project No. 2717G8334b and No. 17-52-50080.

APPENDIX A: MAGNETIC MIRROR REFLECTION SYMMETRY

The Hamiltonian of a SFS junction is represented in continuum as

$$\check{H}(\boldsymbol{r}, \varphi) = \check{H}_0(\boldsymbol{r}, \varphi) + \check{H}_{\rm P}(\boldsymbol{r}), \tag{A1}$$

$$\check{H}_0(\boldsymbol{r},\varphi)=\begin{bmatrix}\xi_{\boldsymbol{r}}\hat{\sigma}_0 & \hat{\Delta}_{\boldsymbol{r}}\\ -\hat{\Delta}^*_{\boldsymbol{r}} & -\xi_{\boldsymbol{r}}\hat{\sigma}_0\end{bmatrix}, \tag{A2}$$

$$\check{H}_{\rm P}(\boldsymbol{r})=\begin{bmatrix}\hat{H}_{\rm p}(\boldsymbol{r}) & 0\\ 0 & -\hat{H}^*_{\rm p}(\boldsymbol{r})\end{bmatrix}, \tag{A3}$$

$$\xi_{\boldsymbol{r}}=-\frac{\nabla^2}{2m}-\epsilon_F, \tag{A4}$$

$$\hat{\Delta}_{\boldsymbol{r}}=[e^{i\varphi_L}\Theta(-x)+e^{i\varphi_R}\Theta(x-L)]\Delta i\hat{\sigma}_2, \tag{A5}$$

$$\hat{H}_{\rm p}=\hat{H}_{\rm h}+\hat{H}_{\rm so}+\hat{H}_{\rm i}, \tag{A6}$$

$$\hat{H}_{\rm h}(\boldsymbol{r})=-\boldsymbol{h}\cdot\hat{\boldsymbol{\sigma}}\,\Theta(x)\,\Theta(L-x), \tag{A7}$$

$$\hat{H}_{\rm so}(\boldsymbol{r})=-i\lambda(\partial_y\hat{\sigma}_1-\partial_x\hat{\sigma}_2)\Theta(x)\,\Theta(L-x), \tag{A8}$$

$$H_{\rm i}(\boldsymbol{r})=\sum_{\boldsymbol{r}_i}v_{\boldsymbol{r}_i}\,\hat{\sigma}_0\delta(\boldsymbol{r}-\boldsymbol{r}_i). \tag{A9}$$

The BdG equation reads

$$[\check{H}_0(\boldsymbol{r},\varphi)+\check{H}_{\rm P}(\boldsymbol{r})]f(\boldsymbol{r},\varphi)=E(\varphi)f(\boldsymbol{r},\varphi), \tag{A10}$$

where E is the eigenenergy depending on the phase difference between the two superconductors $\varphi=\varphi_L-\varphi_R$ and $f(\boldsymbol{r},\varphi)$ is the eigenfunction. The Josephson current is calculated by $J(\varphi)=e\partial_\varphi E(\varphi)$. The transformation of $\varphi\to-\varphi$ is realized by applying the complex conjugation to the Hamiltonian. The BdG equation becomes

$$[\check{H}_0(\boldsymbol{r},-\varphi)+\check{H}^*_{\rm P}(\boldsymbol{r})]f^*(\boldsymbol{r},\varphi)=E(\varphi)f^*(\boldsymbol{r},\varphi). \tag{A11}$$

When the potential satisfies

$$\hat{H}_{\rm P}(\boldsymbol{r})=\hat{H}^*_{\rm P}(\boldsymbol{r}), \tag{A12}$$

we find that $E(\varphi)=E(-\varphi)$ and that $f^*(\boldsymbol{r},\varphi)$ is the eigenfunction belonging to $E(-\varphi)$. The phase shift of such junction is limited to be either $\varphi_0=0$ or π because the Josephson current is an odd function of φ.

The potentials in this paper are represented as

$$H_{\rm p}=h_z\hat{\sigma}_3-i\lambda\partial_y\sigma_1+i\lambda\partial_x\sigma_2+H_{\rm i}(\boldsymbol{r}), \tag{A13}$$

$$H^*_{\rm p}=h_z\hat{\sigma}_3+i\lambda\partial_y\sigma_1+i\lambda\partial_x\sigma_2+H_{\rm i}(\boldsymbol{r}). \tag{A14}$$

Although the second term changes it sign under the complex conjugation, the additional transformation $y\to-y$ cancels the sign changing:

$$H^*_{\rm p}(x,-y)=h_z\hat{\sigma}_3-i\lambda\partial_y\sigma_1+i\lambda\partial_x\sigma_2+H_{\rm i}(x,-y). \tag{A15}$$

In the absence of impurity potential $\hat{H}_{\rm i}(\boldsymbol{r})=0$,

$$\hat{H}^*_{\rm P}(x,-y)=\hat{H}_{\rm P}(x,y) \tag{A16}$$

is satisfied. Such symmetry of the Hamiltonian is called MMR symmetry with respect to the xz plane. The BdG equation in such case,

$$\check{H}(\boldsymbol{r},-\varphi)f^*(x,-y,\varphi)=E(\varphi)f^*(x,-y,\varphi), \tag{A17}$$

indicates that $f^*(x,-y,\varphi)$ is the eigenfunction belonging to $E(-\varphi)$ and that $E(\varphi)=E(-\varphi)$ holds true. As a result, the phase shift φ_0 in Eq. (17) is either 0 or π in the presence of MMR symmetry. This conclusion, however, depends on the direction of magnetic moments. It is easy to confirm that the magnetic moment in the x direction $h_x\hat{\sigma}_1$ in Eq. (A7) preserves MMR symmetry, whereas that in the y direction $h_y\hat{\sigma}_2$ breaks MMR symmetry. Indeed, a paper [29] demonstrated that the junction with the Zeeman filed in the y direction is responsible for φ_0 phase shift in Eq. (17) even in the ballistic limit.

The impurity potential breaks MMR symmetry because of $H_{\rm i}(x,-y)\neq H_{\rm i}(x,y)$ due to its random nature. In the presence of impurities, therefore, the energy of a junction becomes $E(\varphi)\neq E(-\varphi)$. Thus we conclude that a Josephson junction with a particular impurity configuration is the φ_0 junction and the phase shift φ_0 depends on the microscopic potential configuration. When we average the Josephson current over a number of samples with different random configuration, the φ_0 in the averaged Josephson current $\langle J(\varphi)\rangle$ becomes zero. The average of the junction energy satisfies $\langle E(\varphi)\rangle=\langle E(-\varphi)\rangle$ because $\langle H_{\rm i}(\boldsymbol{r})\rangle$ is independent of $\boldsymbol{r}$. Namely, the ensemble average of the Hamiltonian recovers MMR symmetry.

At the end of this section, we discuss an incomplete point in the argument above. It is possible to show that the φ_0 is either 0 or π when Eq. (A12) is satisfied. However, the relation

$$\hat{H}_{\rm P}(\boldsymbol{r})\neq\hat{H}^*_{\rm P}(\boldsymbol{r}) \tag{A18}$$

is only a necessary condition for the φ_0-junction. In the case of a SFS junction consisting of a uniform ferromagnet, for instance, $\hat{H}_{\rm P}=h\hat{\sigma}_2$ is not equal to its complex conjugation. But it is well known that such an SFS junction is either 0- or π-junction. By applying a unitary transformation rotating spin space, the Hamiltonian is transformed to $\hat{H}_{\rm P}=h\hat{\sigma}_3$ which satisfies Eq. (A12). Thus our argument may depend on the gauge choice. Only we know that the sign change of the second term in Eq. (A14) cannot be removed by any rotation

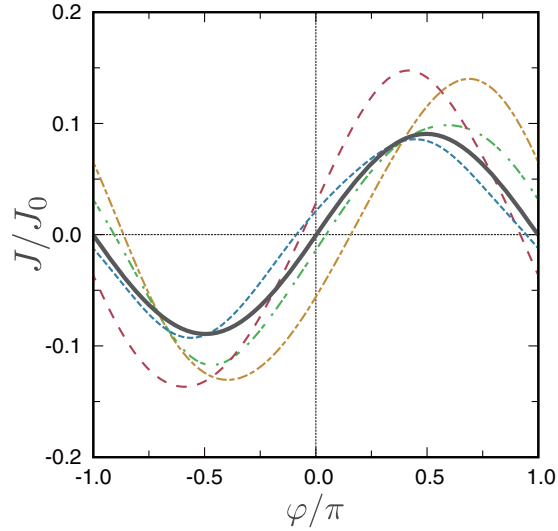

FIG. 11. The current-phase relationships are shown for several samples with different impurity configuration at $h=0.5t$ and $\lambda=0.5t$. The Josephson current after ensemble averaging are plotted by a thick line.

in spin space. Moreover, the argument cannot be applied straightforwardly to superconductors breaking time-reversal symmetry and odd-parity spin-triplet superconductors.

APPENDIX B: NUMERICAL RESULTS FOR A SINGLE SAMPLE

In the dirty regime, calculated results for a single sample can be different from those of ensemble average. Here we present several results before ensemble averaging.

In Fig. 11, we show the CPR at $h = 0.5t$ and $\lambda = 0.5t$. The broken lines are the results calculated for several samples with different random configuration and deviate the sinusoidal function. A thick line corresponds to the ensemble average and is sinusoidal.

Figure 12 shows the spatial profile of the pairing function at $h_z = 0.5t$. The results of ensemble average are shown in Fig. 9. All the components oscillate aperiodically in real space due to the random impurity potential. The opposite-spin components f_0 and f_3 change their sign, whereas the equal-spin components $f_{\sigma,\sigma}$ do not change their sign. Thus, the results suggest the stability of equal-spin pairs in a single sample.

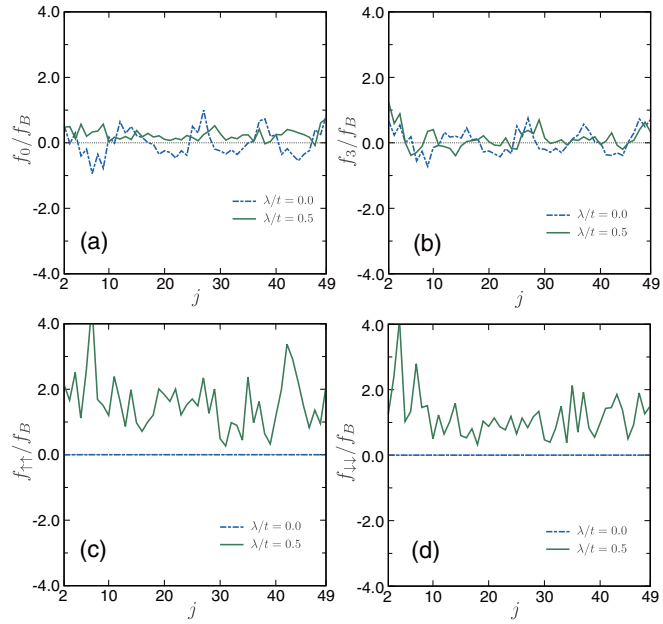

FIG. 12. The spatial profile of the pairing function in a single sample.

[1] L. N. Bulaevskii, V. V. Kuzii, and A. A. Sobyanin, JETP Lett. **25**, 290 (1977).
[2] A. I. Buzdin, L. N. Bulaevskii, and S. V. Panyukov, JETP Lett. **35**, 178 (1982).
[3] F. S. Bergeret, A. F. Volkov, and K. B. Efetov, Phys. Rev. Lett. **86**, 4096 (2001).
[4] A. A. Golubov, M. Y. Kupriyanov, and E. Il'ichev, Rev. Mod. Phys. **76**, 411 (2004).
[5] V. V. Ryazanov, V. A. Oboznov, A. Y. Rusanov, A. V. Veretennikov, A. A. Golubov, and J. Aarts, Phys. Rev. Lett. **86**, 2427 (2001).
[6] T. Kontos, M. Aprili, J. Lesueur, F. Genêt, B. Stephanidis, and R. Boursier, Phys. Rev. Lett. **89**, 137007 (2002).
[7] F. S. Bergeret, A. F. Volkov, and K. B. Efetov, Rev. Mod. Phys. **77**, 1321 (2005).
[8] R. S. Keizer, S. T. B. Goennenwein, T. M. Klapwijk, G. Miao, G. Xiao, and A. Gupta, Nature (London) **439**, 825 (2006).
[9] M. S. Anwar, F. Czeschka, M. Hesselberth, M. Porcu, and J. Aarts, Phys. Rev. B **82**, 100501(R) (2010).
[10] T. S. Khaire, M. A. Khasawneh, W. P. Pratt, and N. O. Birge, Phys. Rev. Lett. **104**, 137002 (2010).
[11] J. W. A. Robinson, J. D. S. Witt, and M. G. Blamire, Science **329**, 59 (2010).
[12] Y. Asano, Y. Tanaka, and A. A. Golubov, Phys. Rev. Lett. **98**, 107002 (2007).
[13] V. Braude and Y. V. Nazarov, Phys. Rev. Lett. **98**, 077003 (2007).
[14] M. Eschrig and T. Löfwander, Nat. Phys. **4**, 138 (2008).
[15] M. Eschrig, Rep. Prog. Phys. **78**, 104501 (2015).
[16] H. Irie, Y. Harada, H. Sugiyama, and T. Akazaki, Phys. Rev. B **89**, 165415 (2014).
[17] H. Takayanagi, T. Akazaki, and J. Nitta, Phys. Rev. Lett. **75**, 3533 (1995).
[18] A. F. Volkov and H. Takayanagi, Phys. Rev. Lett. **76**, 4026 (1996).
[19] T. Nakamura, L. D. Anh, Y. Hashimoto, Y. Iwasaki, S. Ohya, M. Tanaka, and S. Katsumoto, J. Phys.: Conf. Ser. **969**, 012036 (2018).
[20] T. Nakamura, L. D. Anh, Y. Hashimoto, S. Ohya, M. Tanaka, and S. Katsumoto, Phys. Rev. Lett. **122**, 107001 (2019).
[21] E. A. Demler, G. B. Arnold, and M. R. Beasley, Phys. Rev. B **55**, 15174 (1997).
[22] I. V. Krive, L. Y. Gorelik, R. I. Shekhter, and M. Jonson, Low Temp. Phys. **30**, 398 (2004).
[23] A. Buzdin, Phys. Rev. Lett. **101**, 107005 (2008).
[24] Y. Asano and Y. Tanaka, Phys. Rev. B **87**, 104513 (2013).
[25] X. Liu, J. K. Jain, and C.-X. Liu, Phys. Rev. Lett. **113**, 227002 (2014).
[26] F. S. Bergeret and I. V. Tokatly, Phys. Rev. Lett. **110**, 117003 (2013).
[27] F. S. Bergeret and I. V. Tokatly, Phys. Rev. B **89**, 134517 (2014).
[28] F. S. Bergeret and I. V. Tokatly, Europhys. Lett. **110**, 57005 (2015).
[29] T. Yokoyama, M. Eto, and Y. V. Nazarov, Phys. Rev. B **89**, 195407 (2014).
[30] S. H. Jacobsen and J. Linder, Phys. Rev. B **92**, 024501 (2015).
[31] S. H. Jacobsen, J. A. Ouassou, and J. Linder, Phys. Rev. B **92**, 024510 (2015).
[32] J. Arjoranta and T. T. Heikkilä, Phys. Rev. B **93**, 024522 (2016).
[33] A. Costa, P. Högl, and J. Fabian, Phys. Rev. B **95**, 024514 (2017).

[34] S. Mironov and A. Buzdin, Phys. Rev. Lett. **118**, 077001 (2017).
[35] K. Sakurai, S. Ikegaya, and Y. Asano, Phys. Rev. B **96**, 224514 (2017).
[36] H. T. Simensen and J. Linder, Phys. Rev. B **97**, 054518 (2018).
[37] R. M. Lutchyn, J. D. Sau, and S. Das Sarma, Phys. Rev. Lett. **105**, 077001 (2010).
[38] Y. Oreg, G. Refael, and F. von Oppen, Phys. Rev. Lett. **105**, 177002 (2010).
[39] P. A. Lee and D. S. Fisher, Phys. Rev. Lett. **47**, 882 (1981).
[40] Y. Asano, Phys. Rev. B **63**, 052512 (2001).
[41] F. S. Bergeret, A. F. Volkov, and K. B. Efetov, Phys. Rev. B **64**, 134506 (2001).
[42] F. S. Bergeret, A. F. Volkov, and K. B. Efetov, Phys. Rev. B **75**, 184510 (2007).
[43] Y. Asano, Y. Sawa, Y. Tanaka, and A. A. Golubov, Phys. Rev. B **76**, 224525 (2007).
[44] P. A. Ioselevich, P. M. Ostrovsky, Y. V. Fominov, and M. V. Feigel'man, Phys. Rev. B **95**, 094508 (2017).
[45] F. Konschelle, I. V. Tokatly, and F. S. Bergeret, Phys. Rev. B **92**, 125443 (2015).
[46] G. Eilenberger, Z. Phys. A **214**, 195 (1968).
[47] N. Kopnin, *Theory of Nonequilibrium Superconductivity* (Oxford University Press, New York, 2001).
[48] P. Fulde and R. A. Ferrell, Phys. Rev. **135**, A550 (1964).
[49] A. I. Larkin and Y. N. Ovchinnikov, Sov. Phys. JETP **20**, 762 (1965).
[50] Y. Asano, A. A. Golubov, Y. V. Fominov, and Y. Tanaka, Phys. Rev. Lett. **107**, 087001 (2011).
[51] S.-I. Suzuki and Y. Asano, Phys. Rev. B **89**, 184508 (2014).